Polymer 55 (2014) 979–988

Contents lists available at ScienceDirect

Polymer

journal homepage: www.elsevier.com/locate/polymer

Feature article

Computational strategies for polymer dielectrics design

C.C. Wang [a,b], G. Pilania [c], S.A. Boggs [b], S. Kumar [d], C. Breneman [e], R. Ramprasad [a,b,*]

[a] Department of Materials Science and Engineering, University of Connecticut, 97 North Eagleville Road, Storrs, CT 06269, USA
[b] Institute of Materials Science, University of Connecticut, 97 North Eagleville Road, Storrs, CT 06269, USA
[c] Materials Science and Technology Division, Los Alamos National Laboratory, Los Alamos, NM 87545, USA
[d] Department of Chemical Engineering, Columbia University, 500W. 120th St., New York, NY 10027, USA
[e] Rensselaer Exploratory Center for Cheminformatics Research and Department of Chemistry and Chemical Biology, Rensselaer Polytechnic Institute, Troy, NY 12180, USA

ARTICLE INFO

Article history:
Received 23 November 2013
Received in revised form
25 December 2013
Accepted 29 December 2013
Available online 14 January 2014

Keywords:
Computation polymer dielectrics

ABSTRACT

The present contribution provides a perspective on the degree to which modern computational methods can be harnessed to guide the design of polymeric dielectrics. A variety of methods, including quantum mechanical *ab initio* methods, classical force-field based molecular dynamics simulations, and data-driven paradigms, such as quantitative structure–property relationship and machine learning schemes, are discussed. Strategies to explore, search and screen chemical and configurational spaces extensively are also proposed. Some examples of computation-guided synthesis and understanding of real polymer dielectrics are also provided, highlighting the anticipated increasing role of such computational methods in the future design of polymer dielectrics.

1. Introduction

Polymers offer a nearly infinite variety of material systems with diverse properties. Until recently, the formulation of polymers for specific applications was based on trial and error, guided by intuition. The purpose of the present contribution is to demonstrate the degree to which computational methods can guide the design of polymers, in the present case for dielectric applications [1–12], which require high dielectric constant, large band gap, high dielectric strength, low dielectric loss, and appropriate glass transition temperature and morphology.

At the most fundamental level, computational quantum mechanics, e.g., density functional theory (DFT), can be used to determine properties of dielectrics at the scale of a crystalline unit cell [13–17]. Such properties include structural and thermodynamic details, reasonable estimates of the band gap, electronic dielectric constant, ionic dielectric constant, and intrinsic breakdown field [18–24]. In addition, impurity states in the band gap caused by common chemical impurities can be computed [25–28]. Realistic models can also be developed for metal–polymer interfaces in order to predict charge injection characteristics.

Larger scale morphological features of polymers can be accessed practically at the present time only using molecular dynamics (MD) based on empirical interatomic potentials or force fields [29–33]. Such simulations can predict crystal structure, semicrystalline morphology and provide rough estimates of glass transition temperature and dielectric loss, although the latter is presently limited to loss in the GHz range [34–37].

The above methods can be classified as “physics-based”, as they are based on quantum mechanics, classical mechanics, and classical electromagnetism. An emerging class of methods, often referred to as “data-driven”, use various forms of multivariate analysis on experimental or computational data, based on complex variables with a physical relationship to the properties being predicted [38–46]. Such systems are “trained” on available data and then used to predict properties of interest for polymers for which data are not available. An example of such data-driven approaches is quantitative structure property relationships (QSPR) [47–51], which can predict properties, such as glass transition temperature, melting temperature, etc., for which no fundamental approach is presently available.

In this contribution, we provide a perspective on the application of modern computational approaches to the design of polymeric dielectrics. Section 2 addresses functionalization of a well-understood polymeric dielectrics, such as polyethylene (PE) and polypropylene (PP), to enhance its dielectric response. Section 3 discusses approaches to the discovery of entirely new classes of polymer dielectrics, both organic and organometallic. Strategies discussed include exploration of large chemical spaces and efficient computation of some relevant properties. The proper starting point

* Corresponding author. Department of Materials Science and Engineering, University of Connecticut, 97 North Eagleville Road, Storrs, CT 06269, USA.
E-mail addresses: rampi@ims.uconn.edu, rampi@uconn.edu (R. Ramprasad).

0032-3861/$ – see front matter © 2014 Elsevier Ltd. All rights reserved.
http://dx.doi.org/10.1016/j.polymer.2013.12.069

for such chemical space exploration is a quantum mechanics based method such as DFT, but the promising systems identified using quantum mechanics must be investigated using other methods that treat the morphology (e.g., force field based MD), glass transition temperature (QSPR), melting temperature (QSPR), etc. The screening of systems considered in Section 3 is based on dielectric constant and band gap. Appropriate values for these properties are "necessary but not sufficient" for a given application and, therefore, appropriate for first-level screening. After the first-level screening for these properties, promising candidates can be subjected to more detailed analysis for a broader range of properties required for a given application. These include factors that control the injection of charge carriers from a metal electrode into the polymer, formation of defect states in the polymer, factors that control the transport of charge carriers (e.g., scattering due to dipoles, impurities and phonons), dielectric breakdown, glass transition temperature, etc. Such aspects are discussed in Section 4. The role data-driven approaches, such as QSPR and, in particular, the emerging area of "machine learning", is surveyed in Section 5. We conclude with our outlook in Section 6.

2. Modification of existing polymer dielectrics

A good place to start in applying computational methods to design new materials is to understand or identify the factors that lead to surprising properties when a well-studied material is modified creatively. Polypropylene (PP), in its biaxially oriented form, is the most common polymer dielectric for high energy density capacitors as a result of its high dielectric breakdown strength, low dielectric loss, and good clearing characteristics; however, its dielectric constant is only 2.2 [52–54]. Increasing the dielectric constant while maintaining or improving other properties, such as operating temperature range, is highly desirable. Chung has developed an –OH functionalized PP which doubles the dielectric constant and maintains relatively low loss with only 4.2 mol% –OH (Fig. 1) [55–57]. The experimental data also imply that the PP–OH contains roughly 0.5 water molecule per –OH moiety on the chain and that the –OH groups are hydrogen-bonded in pairs.

DFT computations can investigate the role played by –OH functional groups and the trapped moisture [59]. Given that DFT computations are time-intensive, two short-chain polyethylene oligomers (o-PE), each with 11 carbon atoms, were considered. This o-PE system is chemically similar to PP, but much simpler and

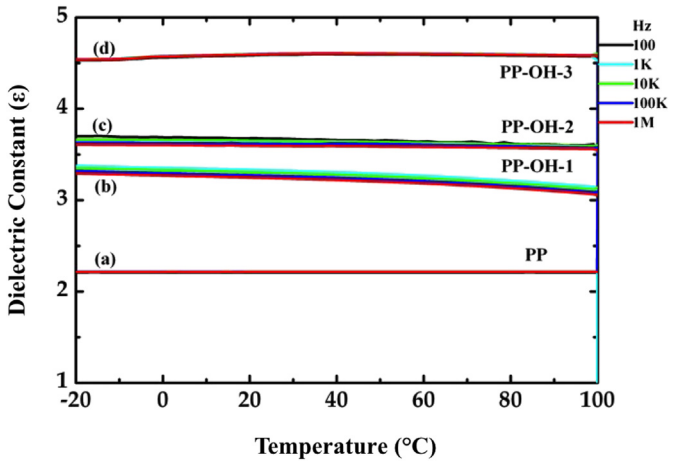

Fig. 1. Dielectric constants (vs. frequency and temperature) for (a) polypropylene (PP) and three hydroxyl (–OH) functionalized PP (PP–OH) copolymers containing (b) 0.7, (c) 1.8, and (d) 4.2 mol% OH content. Replotted from data in Ref. [55].

smaller in size. The two chains were arranged in a head-to-tail configuration, and an H chain end atom was substituted by an –OH group (o-PE–OH). Additionally, to explore the effect of water molecules, o-PE–OH with one and two water molecules (o-PE–OH–H_2O and o-PE–OH–$2H_2O$, respectively) were studied. Fig. 2 shows snapshots of the optimized geometries. The average value of the total dielectric constant, i.e., the trace of the dielectric constant tensor, including both ionic and electronic contributions, for the o-PE, o-PE–OH, o-PE–OH–H_2O, and o-PE–OH–$2H_2O$ systems were, respectively, 2.4, 3.3, 3.7, and 4.3 (Fig. 3) [59]. The determination of the dielectric constant of such chain systems was performed using a recently developed method aimed at precisely these situations [19]. For pure PE, the dielectric constant, which is almost entirely due to electronic contributions, is close to the accepted experimental value. The increase in the dielectric constant due to the –OH groups (without and with water molecules) is caused entirely by the ionic contributions. The proper account of van der Waals (vdW) interactions [60,61], secondary bonding phenomena such as H-bonding, etc., is captured adequately in the DFT computations. For instance, Fig. 2(d) shows the relaxed geometry of the o-PE–OH–$2H_2O$ system, where the formation of an H-bonded ring containing two –OH groups and $2H_2O$ molecules, is evident.

While the DFT computations provide some understanding of the role played by –OH functional groups and the accompanying water molecules, these data are qualitative. The DFT analysis ignores complexities associated with morphological variations of PE when functionalized with –OH, and owing to computational considerations, the concentration of –OH modeled is much greater than in experiments. Large-scale MD simulations based on force fields are required to address morphological aspects of the system at realistic –OH concentrations. Recent force-field based MD simulations have extended the DFT work discussed above [62]. In the MD simulations, PE–OH with 4.2 mol% –OH groups was considered, and varying amounts of water were added into PE-OH system. The morphology of –OH groups, trapped water and H-bonding was well captured, insofar as can be concluded by comparisons with measured infrared spectra. In addition, the MD simulations indicate that the –OH groups tend to collect at amorphous–crystalline interfaces, likely as a result of –OH groups "expelled" from the crystalline regions during formation. These simulations also imply that hydrogen bonding of the –OH groups into pairs is essential to maintaining low dielectric loss. Fig. 3 summarizes data for the dielectric constant derived from the MD simulations, in addition to the results from DFT computations and experiment. The addition of water results in a significant increase in dielectric constant. For ~0.5 water per –OH group, the MD data for dielectric constant match closely the experimental value of ~3.4, and larger amounts of water, so long as they are "trapped" by the –OH groups much like in Fig. 2(d), increase the dielectric constant further without increasing loss.

The DFT, MD and experimental data, collectively, have allowed us to understand the factors that lead to a significant increase in the dielectric constant of a saturated hydrocarbon due to the incorporation of a small amount of –OH groups. These findings are significant, as they imply a path toward tunable control of dielectric properties of polyolefins through functionalization. While the analysis presented underlines the complexities that can result from incorporation of a functional group, it also demonstrates the utility of computational strategies for systematic studies of other functional groups.

3. Pathways to the discovery of new polymer dielectrics

While modifying an existing polymer to enhance its properties is a promising approach and offers a "risk mitigation" strategy,

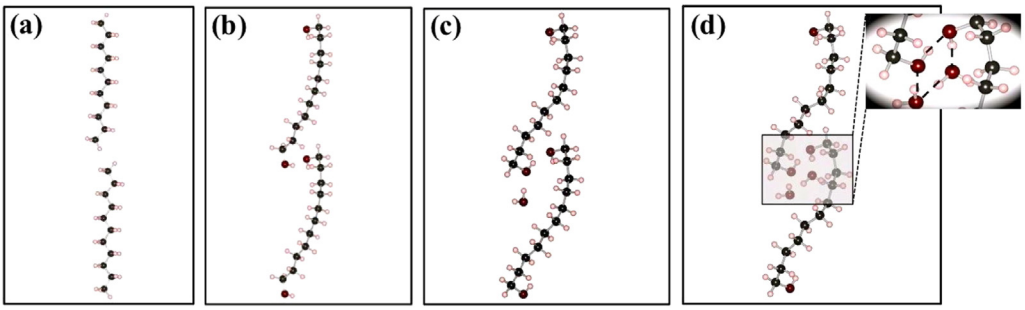

Fig. 2. Optimized structures of (a) o-PE, (b) o-PE–OH, (c) o-PE–OH–H_2O, and (d) o-PE–OH–$2H_2O$. Black, white, and red spheres represent C, H, and O atoms, respectively. The inset shows a typical hydrogen bonded ring.

identifying or discovering entirely new classes of polymers can be transformative but requires systematic schemes to explore the polymer chemical space. Fig. 4 portrays one such scheme in which single polymeric chains consist of four distinct building blocks drawn from a pool of possibilities in a combinatorial manner [19,20]. Depending on the pool of blocks, various polymer classes can be studied. The combinatorial explosion produced by this strategy is both a blessing and a curse. For example, 10 possibilities for each of the 4 blocks in the repeat unit result in a total of 10,000 cases, although translational and inversion invariances, and other considerations such as chemical intuition, can reduce this number considerably.

3.1. New organic polymers

We first consider a set of organic building blocks, for example, –CH_2–, –NH–, –C(=O)–, –C_6H_4– (benzene), –C_4H_2S– (thiophene), –C(=S)–, and –O– [63,64], which are common in polymer backbones and various combinations of which form traditional polymers, including polyesters, polyamides, polyethers, polyureas, etc. Accounting for translational and inversion symmetries, and removing unstable systems, leaves 267 symmetry-unique systems.

The two most important properties of dielectrics for most applications are dielectric constant and band gap. Hence, we focus on these two properties in this section. With the aid of a recently developed method which determines the dielectric constant of such single chain systems [19], high throughput DFT computations can be used to obtain the band gap and dielectric constant of the 267 polymer systems. Fig. 5(a)–(c), respectively, shows the relationship between the electronic, ionic and total dielectric constant and band gap for the 267 polymer systems. A near perfect inverse Pareto optimal front relationship between the band gap and the electronic dielectric constant can be seen from Fig. 5(a), which imposes a theoretical limit on the electronic part of the dielectric constant as a function of band gap, a limit that can be understood by regarding the electronic part of the dielectric response as a sum over electronic transitions from occupied to unoccupied states. On the other hand, the ionic dielectric constant is not correlated with the band gap, as seen from Fig. 5(b). The ionic contribution is determined by the infrared active zone center phonon modes (i.e., the modes that display a time-varying dipole moment) [65,66].

The ionic dielectric constant can thus be exploited to increase the total dielectric constant without compromising the band gap. Fig. 5(c) shows the variation of the total dielectric constant with the band gap. Plots such as Fig. 5(c) provide us with a "map" of the achievable combination of properties within the chemical space explored. Capacitive energy storage and some electronics applications, e.g., gate insulations, could draw from the large dielectric constant and moderate band gap region of this plot. Desirable material properties are likely to be associated with certain building block structures. Such observations could accelerate the design process by identifying correlations between material properties and specific building blocks structures. Indeed, guided by the DFT results, a few polyureas and polyurethanes containing –NH–, –C(=O)–, –C_6H_4–, and –O– building blocks have been synthesized using step polymerization [64].

Once a set of promising polymers has been identified, their crystal structures and morphologies must be investigated. If interatomic potentials are available to handle the systems, MD simulations can be used to determine their crystal structure and

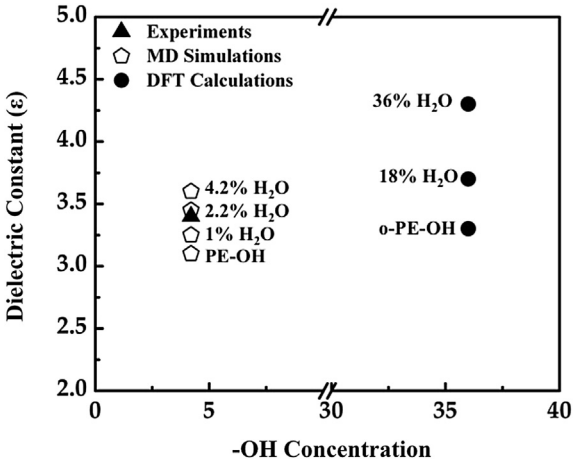

Fig. 3. Comparison of the dielectric constant of hydroxyl functionalized polyethylene (PE–OH), obtained from experiment, MD simulations and DFT calculations.

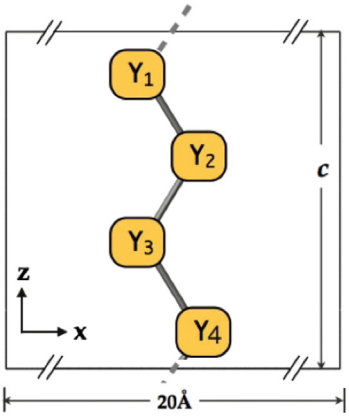

Fig. 4. Schematic representation of the polymeric chain model. *c* is the lattice constant along the polymer chain direction that was allowed to relaxed along with the internal coordinates. Four blocks Y_1, Y_2, Y_3, and Y_4 can be filled up by different motifs.

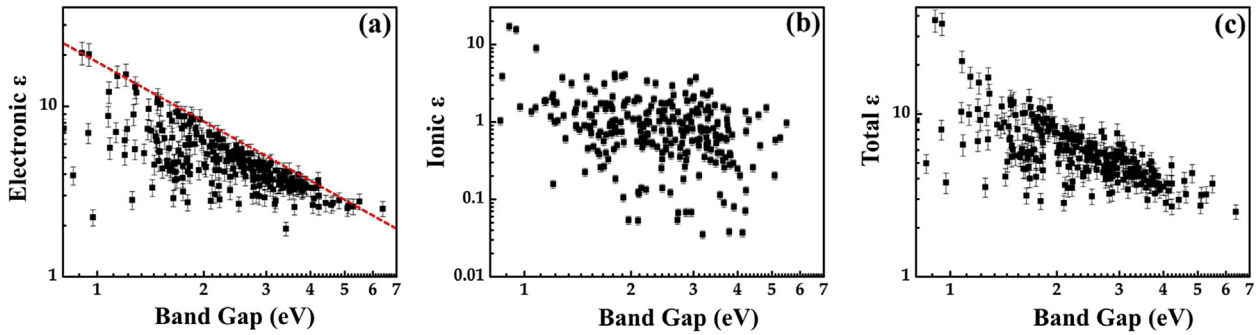

Fig. 5. (a) Electronic, (b) ionic and (c) total dielectric constant (ε) as a function of the band gap, for the class of organic polymers considered, computed using DFT within the single-chain approach. The building blocks were drawn from the following pool of possibilities: $-CH_2-$, $-NH-$, $-C(=O)-$, $-C_6H_4-$ (benzene), $-C_4H_2S-$ (thiophene), $-C(=S)-$, and $-O-$. The axes are in logarithmic scale.

morphology, for example, using a melt and quench approach [34–37]. An additional option, especially if force fields are not available for the new identified systems, is to use 3-dimensional structure searching schemes [67–72] to determine the ground state structures based on DFT.

3.2. Polymer blocks containing group 14 elements

The strategy described above can be extended by considering building units based on non-carbon elements from Group 14 of the periodic table, i.e., Si, Ge and Sn. Replacing C with Si, Ge or Sn offers the opportunity to manipulate the band gap and the electronic part of the dielectric constant through control of σ conjugation along the chain, and to manipulate the ionic part of the dielectric constant through control of dipole moments. Substituting C with Si, Ge and/or Sn ensures chemical compatibility by preserving the local chemical environment and bonding. The dipole moments of each building block can be enhanced by introducing small atoms with high electronegativity such as F and Cl to the side chain. We thus consider polymers with building block units represented as $-XY_2-$ in this section, where X = C, Si, Ge, Sn and Y = H, F, Cl.

Before exploring the single chain systems based on the above combinatorial exercise, we investigate $-XY_2-$ "homopolymer" crystals to see if any pattern emerges. Group 14 systems display rich chemistry and crystallize in forms with differing coordination geometries. While C always prefers a 4-fold coordination environment, Ge favors a 5-fold environment, and Sn can occur in 6 or 7 fold coordination geometries [19,73]. Fig. 6 presents dielectric constant and band gap data for homopolymer ground state geometries. The electronic part of the dielectric constant tends to vary inversely with the band gap, as expected, while the ionic contribution to the dielectric constant is negligible for the C based systems, low for the Si based systems, but quite high for the Ge and Sn containing polymers. Fig. 6 also reveals that $-XY_2-$ homopolymers with Ge and Sn backbone have large dielectric constants but smaller band gaps than C and Si-based polymers [19,73]. Pure PE has a large band gap but relatively small dielectric constant. A natural next step is to "mix" PE with the $-XY_2-$ homopolymers to identify compositions which span a large range of band gap and dielectric constant. Such a combinatorial exploration based on the scheme presented in Fig. 4 involving 7 building block possibilities (namely, $-CH_2-$, $-SiF_2-$, $-SiCl_2-$, $-GeF_2-$, $-GeCl_2-$, $-SnF_2-$ and $-SnCl_2-$) was recently undertaken [20,38]. Results for dielectric constant vs. band gap for the 175 such single chain polymers are shown in Fig. 7. While PE has the greatest calculated band gap of the systems explored, addition of Group 14 elements leads to progressive decrease in the band gap and increase in the electronic dielectric constant. The total dielectric constant of the Group 14 element-based polymers spans over a large range between 2.5 and 47, with the smallest and largest values corresponding to $-(CH_2)_4-$ and $-CH_2-(SnF_2)_3-$, respectively. As the backbone atoms vary from C to Sn with all other units in the chain are held fixed, both the electronic and total dielectric constant increase, as the band gap decreases, probably because $-SnF_2-$ has the largest dipole moment and the Sn–Sn bond rotation has the lowest barrier among all the X–X' (with X or X' = C, Si, Ge, and Sn). Compared with organic polymers, the Group 14 element-based hybrid polymers, especially those involving Sn, can achieve greater dielectric constants without large reductions of the band gap, which makes them attractive candidates for high dielectric constant polymeric dielectrics [20,38].

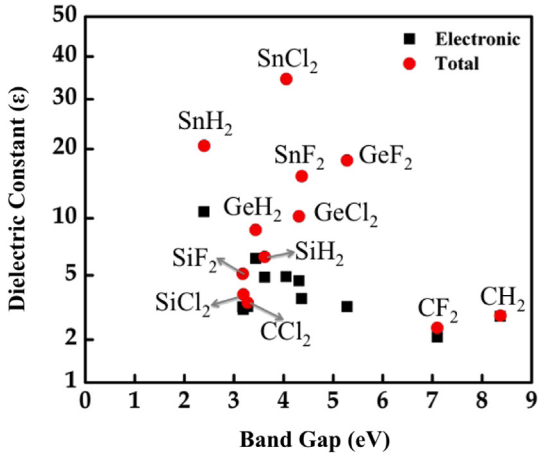

Fig. 6. Dielectric constant and band gap results for $-XY_2-$ homopolymer crystals at their respective ground state structure (where X = C, Si, Ge, Sn and Y = H, F, Cl).

4. Advanced screening strategies

The above discussion dealt largely with dielectric constant and band gap. While these two properties are important, many other factors are relevant to practical applications. Thus down-selection of promising candidates requires estimating a range of other parameters. In the following, we describe briefly a selection of such factors, to highlight the present state-of-the-art in the computation of material properties, and the challenges that need to be overcome.

4.1. Electron/hole injection barriers at metal–polymer interfaces

Electronic and capacitor applications require the polymer dielectric to contact a metal electrode. Such an interface sometimes

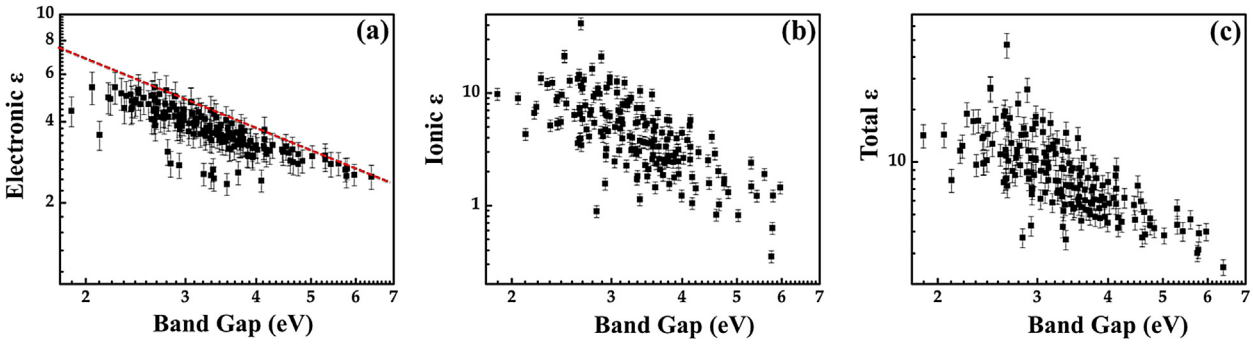

Fig. 7. (a) Electronic, (b) ionic and (c) total dielectric constants (ε) as a function of the band gap, for the class of polymers containing Group 14 elements, computed using DFT within the single-chain approach. The building blocks were drawn from the following pool of possibilities: $-CH_2-$, $-SiF_2-$, $-SiCl_2-$, $-GeF_2-$, $-GeCl_2-$, $-SnF_2-$ and $-SnCl_2-$. The axes are in logarithmic scale.

dominates the performance of polymer dielectrics, as charge injection from the metal electrode to the polymer is the primary source of charge during conduction. The property that determines charge injection at interfaces is the Schottky barrier heights for electron and hole injection, which can be computed using modern DFT. Such issues have been encountered in past studies of metal–dielectric or metal–semiconductor interfaces within the context of (inorganic) semiconductor devices [74–77]. While methods developed earlier can be used within the context of metal–polymer interfaces, the primary impediment to doing so is the complex nature of the metal–polymer interface at the atomic-level, which is far from ideal or "abrupt", unlike interfaces typically encountered by the semiconductor community. Future efforts to compute barrier heights must break new ground in terms of realistic models of interfaces, perhaps through a combination of DFT and force-field based computations.

4.2. Defects in insulating polymers

Chemical impurities in polymer dielectrics introduce localized states in the band gap which can act as traps and thereby affect conduction and high field aging (i.e., the gradual degradation of the dielectric). Previous studies based on DFT provide an understanding of impurity states in the band gap resulting from chemical impurities and conformational distortion [25–28]. While states caused by the latter lie very near to the band edges (the conduction band in particular), those caused by the former tend to be separated from the valence and conduction band edges by $\gtrsim 1$ eV, as shown in Fig. 8. States close to the valence band edge are normally occupied and represent hole traps, while those close to the conduction band are normally empty and represent electron traps. The hole (electron) traps fill when positive (negative) space charge is injected into the material at high field.

Polymer aging occurs over time as a result of thermal, oxidative, mechanical, electrical, etc., effects, and can be caused by the breaking of primary chemical bonds in the chain backbone or side groups. Aging can also cause conformational changes which result in reduced crystallinity. Experimental evidence suggests that high field aging occurs as a result of recombination of electrons and holes as the opposite space charge fields pass through each other [78]. Under repetitive DC charging at sufficiently high fields, carrier recombination can occur at electrodes as a result of voltage cycling, and carrier recombination in the bulk occurs during steady state voltage. In either case, carrier recombination releases sufficient energy to break chemical bonds, which, in the presence of oxygen, can result in carbonyl formation, increased impurity states in the band gap, and enhanced conduction to form a positive feedback loop which eventually leads to breakdown.

A microscopic mechanism governing the initiating step in the high-field aging of crystalline polyethylene has been recently proposed based on DFT calculations and *ab initio* MD simulations [79]. The study assumed that electrons, holes, and excitons are present in the system. The key finding of this work is that the presence of triplet excitons can be damaging. The electron and hole states of the exciton localize on a distorted region of polyethylene and weaken nearby C–H bonds facilitating C–H bond scission. The estimated barrier to cleavage of the weakened C–H bonds is comparable to the thermal energy, suggesting that this mechanism may be responsible for the degradation of polyethylene when placed under electrical field, e.g., in high-voltage cables. Fig. 9 shows a snapshot of this process during the course of a DFT-based MD simulation. Laurent et al. have quantified these phenomena experimentally, to some degree, based on electroluminescence measurements [80].

4.3. Dielectric breakdown

The dielectric breakdown field of a capacitor dielectric is correlated strongly with its energy density (i.e., its energy storage capacity). Although extrinsic factors, e.g., chemical impurities, nano-sized cavities, etc., are important in determining breakdown field for polymer-based dielectrics, a firm theoretical understanding of the factors governing the intrinsic breakdown field is an essential first step in developing a model relevant to practical

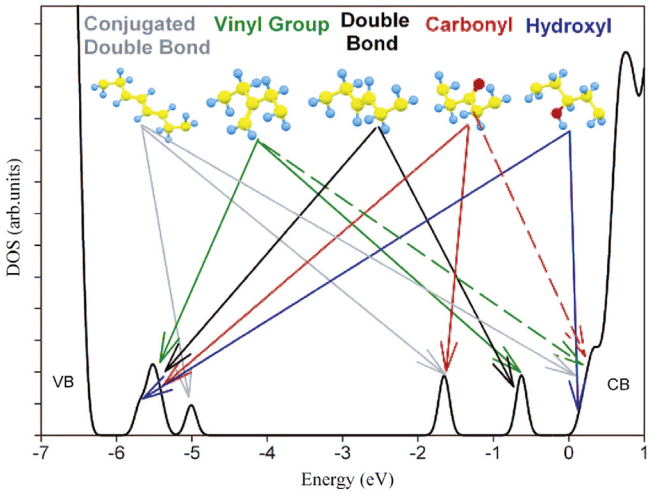

Fig. 8. Density of states for polyethylene showing the impurity states created by a range of common chemical impurities. The zero of energy is referenced to the vacuum level, which is about 0.3 eV below the conduction band minimum of crystalline polyethylene [25].

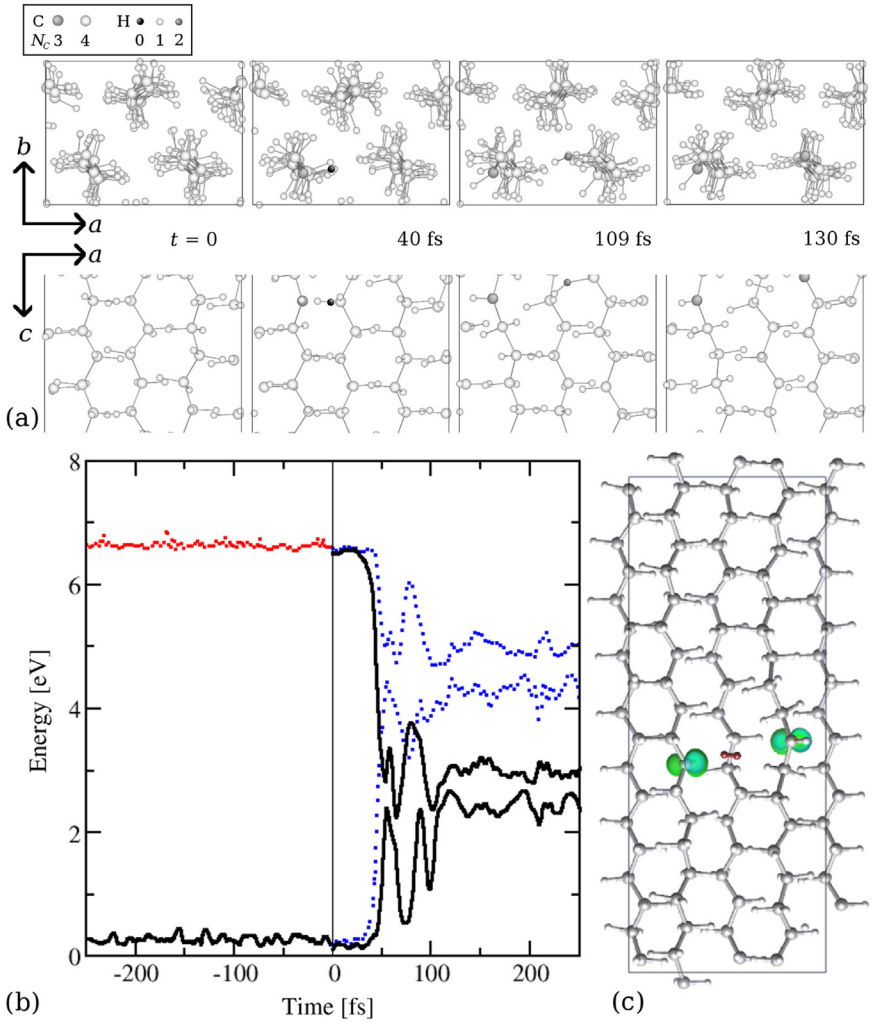

Fig. 9. (a) Snapshots taken at time t during *ab initio* MD simulations of polyethylene, where $t = 0$ refers to the point at which the exciton was injected. Atoms are shaded according to coordination number N_C. The snapshots illustrate C–H bond scission and the subsequent H abstraction. (b) Evolution of the highest occupied and lowest unoccupied energy eigenvalues of the system for 250 fs prior to ($t < 0$) and after ($t > 0$) exciton injection. The zero of energy is the value of the highest occupied PE eigenvalue at $T = 0$. Prior to exciton injection, each of the two levels shown is doubly occupied (the colors shown correspond to spin up states). Upon triplet exciton injection, both hitherto spin-degenerate states split into an occupied spin up (full black lines) and an unoccupied spin down (dotted blue lines) state. (c) Magnetization density plot of the system at $t = 121$ fs. The magnetization is tightly localized on the –CH– groups along the main chains, indicating that these groups have unpaired electrons. The H_2 dimer is shown in deep red for clarity. Reprinted with permission from Ref. [79].

materials. Theories of intrinsic breakdown were developed in the 1930s by Von Hippel [81], Zener [82], and Frohlich [83]. Recently an approach to treat intrinsic breakdown using DFT in the average electron model of Von Hippel has been developed [21,22]. The principal phenomenon governing the intrinsic breakdown field is scattering of conduction-band electrons by phonons, i.e., crystal lattice vibrations. A simple model which reflects the balance between the average energy gain of electrons from the electric field and average energy loss through phonon scattering provides a basis for computing intrinsic breakdown. Upon application of a field smaller than the breakdown field, the average electron energy increases to some stable value at which the rate of energy gain from the field is balanced by energy loss to the lattice. Von Hippel "low energy criterion" defines the breakdown field as that at which the average rate of energy gain is greater than the average rate of energy loss for all energies up to the threshold for impact ionization. At this point, a rapid increase in the density of conduction electrons occurs, which we assume is sufficient to cause breakdown.

Fig. 10 compares the calculated intrinsic breakdown with the maximum experimentally observed breakdown field for a range of ionic and covalent materials [21,22]. Good agreement is achieved in that the computed breakdown field tracks the upper bound of the measured intrinsic breakdown field. Understanding of intrinsic breakdown is reasonably good for crystalline materials, but computation of engineering breakdown fields requires accounting for effects of morphology, chemical impurities, and defects such as nanocavities.

4.4. Glass transition temperature

We now move from electrical properties to an important physical property, the glass transition temperature, T_g. Many properties change dramatically when an amorphous polymer undergoes glass transition. For instance, the dielectric loss of a polar material normally increases dramatically as the polymer goes through its T_g. At temperatures below T_g, polymers are hard and glassy because motion of polymer chains is restricted to local vibration. When the temperature goes to above T_g, chains have greater mobility and the polymer softens. Various factors affect the T_g of polymers, e.g., molecular weight and the chemical structure.

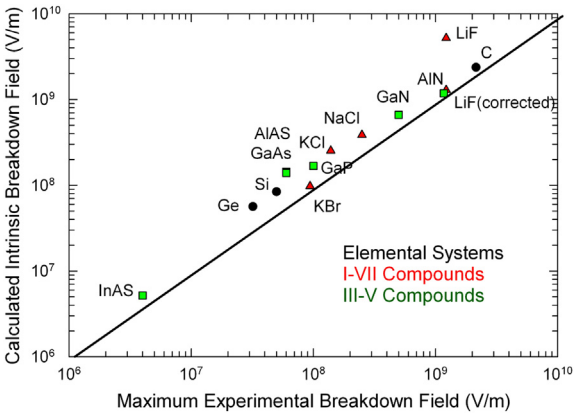

Fig. 10. Comparison of the maximum experimental breakdown field and the calculated intrinsic breakdown field for a range of covalently bonded and ionic materials. In the case of LiF, the enthalpy of formation (6.39 eV) is much lower than the band gap (14.2 eV). Thus bond breakage will occur before impact ionization. The LiF(corrected) is based on using the enthalpy of formation as the impact ionization threshold instead of the band gap. The symbols code for material type (element, etc.) while the text in the figures codes for material structure, i.e., diamond structure: Ge, Si, C; rocksalt structure: KBr, KCl, NaCl, LiF; zincblende structure: InAs, GaAs, GaP, AlAs; wurtzite structure: AlN, GaN [22].

While T_g can be estimated using MD simulations, the cooling and heating rates that can be simulated are much greater than reality. Thus, T_g estimated using MD tends to carry large error bars. A second alternative to computing T_g is provided by Quantitative Structure–Property Relationship (QSPR) methods [47–51]. The philosophy underlying a QSPR study is to relate structural information through descriptors to macroscopic properties. The ability of QSPR to predict the T_g of homopolymers (as well as the polarizabilities, dielectric constants, and HOMO–LUMO gaps of some polymers and functional groups) has already been demonstrated [39]. The polymers were represented using the repeat unit structure, end-capped with a monomer. After selecting the appropriate descriptors, statistical methods were applied to generate linear or nonlinear models. Fig. 11 compares experimental and predicted T_g for two QSPR models and demonstrates the predictive ability of the QSPR models for T_g. The wide structural diversity of the polymers proves that this is a general method for predicting T_g of non-cross-linked polymers which can be used reliably during screening studies.

While QSPR methods cannot generally duplicate the accuracy of physics-based calculations, they are capable of quickly providing remarkably useful results within well-defined domains of applicability when the models are trained using appropriate physics-based descriptors, and are subject to "best practices" model building and validation criteria. Often, the most important determinant for the usefulness of a QSPR model in any design project is whether the domain of applicability of the model can be defined.

5. Advanced searching strategies

DFT-based strategies are limited to polymers based on short, periodic chains. For longer chains required to screen larger regions of compositional space, the computational cost associated with DFT rises rapidly. Furthermore, as the system size increases, the number of candidates within the system grows exponentially, which leads to combinatorial explosion. Take the Group 14 element-based hybrid polymers for example. Doubling the supercell size along the chain direction to include 8 distinct building units in a periodic repeating cell results in a total of 29,365 symmetry unique systems. Clearly, exploration of such a vast chemical space using present first principles based approaches is impractical. A new approach is needed for this large class of systems.

To effect such large scale explorations, a machine learning approach has been developed and applied to the Group 14 element-based hybrid polymers [38]. The initial dataset was generated using the high throughput DFT calculations. To validate the machine learning algorithm, five properties in addition to dielectric constant and band gap were computed, viz., atomization energy, formation

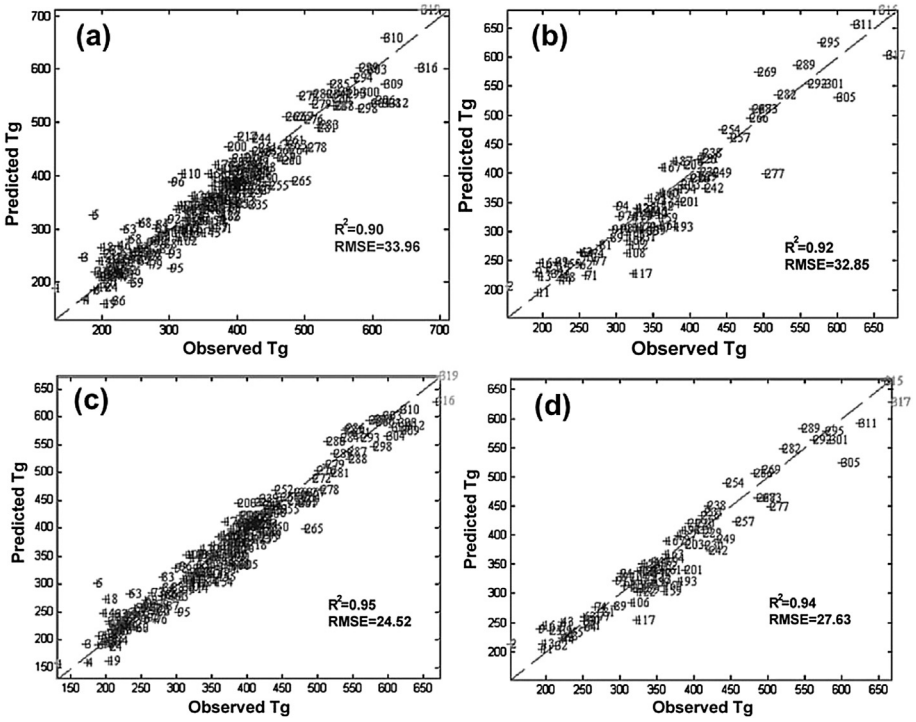

Fig. 11. Partial least square (PLS) model for T_g ((a) training set and (b) test set) and Kernel PLS model for T_g ((c) training set and (d) test set). Reprinted with permission from Ref. [39].

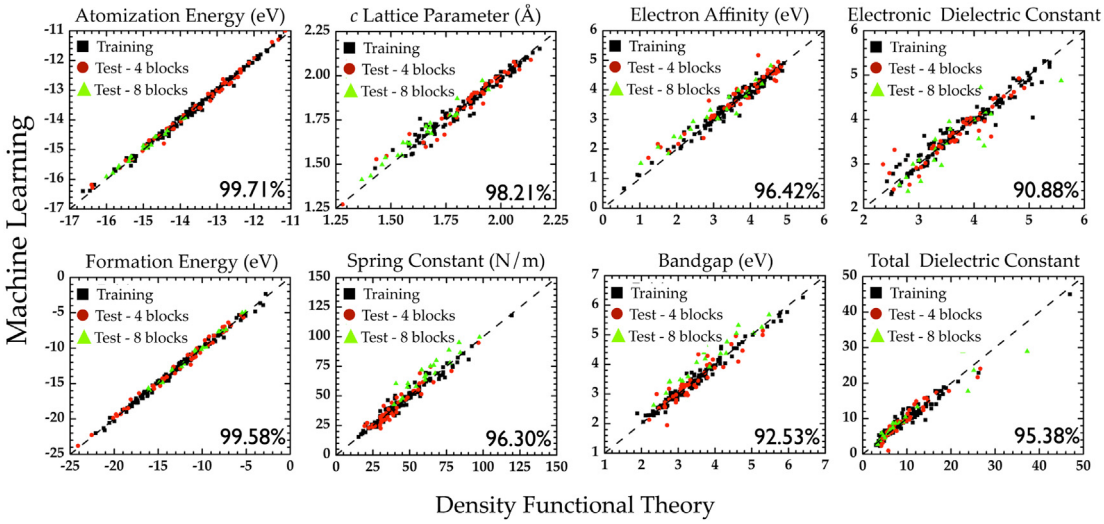

Fig. 12. Parity plots comparing property values computed using DFT against predictions made using learning algorithms trained using chemo-structural fingerprint vectors. Pearson's correlation index is indicated in each of the panels to quantify the agreement between the two schemes [38].

energy, *c* lattice parameter, spring constant, and electron affinity. Fig. 12 shows the agreement between predictions of the model and DFT computations which were separated randomly into "training" and "test" sets, the former used in model development and the latter for validation. Several chains composed of 8-block repeat units, in addition to the 4-block systems portrayed in Fig. 4, were considered. As can be seen, the agreement between the DFT and the learning schemes is uniformly good for all eight properties across the 4-block training and test set, as well as the somewhat out-of-sample 8-block test set. The fidelity of the model predictions is impressive, given that these calculations take a very small fraction of the time required for a typical DFT computation.

While the good agreement between the machine learning and DFT data is gratifying, the real power of this approach lies in the possibility of exploring a much larger chemical space than is practical using DFT calculations or experiments. As mentioned above, expanding the 4-block Group 14 element-based hybrid polymers to 8-blocks results in 29,365 symmetry unique systems. The machine learning approach makes practical a study of this magnitude. Fig. 13 shows the predictions of band gap, electronic and total dielectric constant for the 29,365 systems. The inverse correlation of the band gap with the electronic dielectric constant is confirmed once again from Fig. 13(a). The rough inverse correlation between total dielectric constant and band gap seen in Fig. 13(b) is surprising, although clear deviations from this inverse behavior are seen. This extensive search facilitates identification of candidate polymer dielectrics for various applications. For capacitor applications, a search for polymers with high dielectric constant and large band gap leads to systems in the top part of Fig. 13(b), corresponding to the 'deviations' from the inverse correlation and indicated by a circle in Fig. 13(b). These are systems that contain two or more contiguous SnF_2 units, but with an overall CH_2 mole fraction of at least 25%. Such organo-tin systems may be appropriate for polymer dielectrics. By learning effectively from the available DFT data, the machine learning approach facilitates searching a much larger scale polymer chemical space efficiently. With the aid of this approach, the discovery of new polymer dielectrics can be accelerated significantly.

6. Conclusion

In this contribution, we have surveyed a number of computational methods including classical, quantum mechanical and modern data-driven statistical learning approaches for a theory-

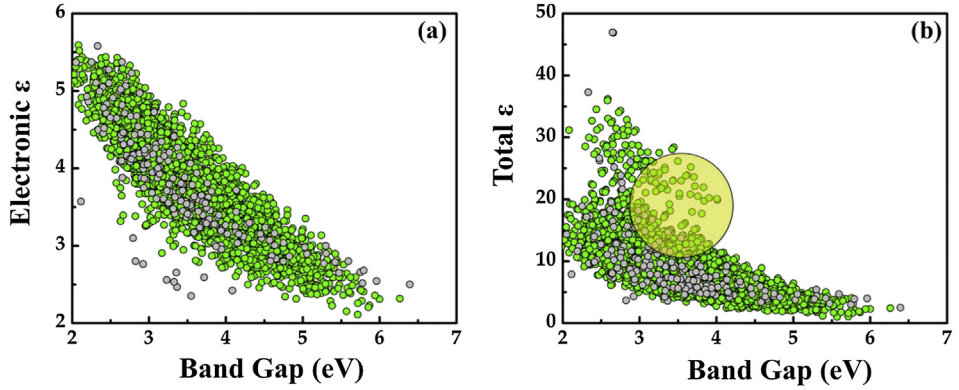

Fig. 13. Machine learning predicted (a) electronic and (b) total dielectric constant as a function of the band gap for the 8-block systems. The DFT results for the 4-block systems (gray circles) are also shown in the figure as comparison. Replotted from data in Ref. [38].

informed rational design of polymeric materials for dielectric and related applications. The examples discussed in this *Perspective* include computational strategies for the modification of existing polymers, as well as the discovery of novel polymer dielectrics and have guided successful experimental results. These success stories clearly demonstrate that carefully devised *in silico* design strategies, which combine computational methods over a range of time and length scales, are now capable of driving experimental studies toward materials of technological interest. Finally, we believe that the overarching ideas and screening strategies described in this paper are quite general and can easily be imported to address materials-related design challenges efficiently in other technological areas.

Acknowledgments

This work was supported by a Multi-University Research Initiative (MURI) grant from the Office of Naval Research, under award number N00014-10-1-0944. Partial computational support of this research was provided by the National Science Foundation through XSEDE resources under Grant No. TG-DMR080058N and the Rensselaer Center for Biotechnology and Interdisciplinary Studies. Helpful discussions with Dr. Daniel Sinkovits, Mr. Arun Mannodi-Kanakkithodi and Dr. Huan Tran are also gratefully acknowledged.

References

[1] Sarjeant WJ, Zirnheld J, MacDougall FW. IEEE Trans Plasma Sci 1998;108:1368–92.
[2] Ho J, Jow R. Characterization of high temperature polymer thin films for power conditioning capacitors. Army Research Laboratories; Jul. 2009. ARL-TR-4880.
[3] Zhu L, Wang Q. Macromolecules 2012;45:2937–54.
[4] Chu B, Zhou X, Ren K, Neese B, Lin M, Wang Q, et al. Science 2006;313:334–6.
[5] Wang Y, Zhou X, Chen Q, Chu BJ, Zhang QM. IEEE Trans Dielectr Electr Insul 2010;17:1036–42.
[6] Wu S, Li WP, Li MR, Burlingame Q, Chen Q, Payzant A, et al. Adv Mater 2013;25:1734–8.
[7] Yoon M-H, Yan H, Facchetti A, Marks TJ. J Am Chem Soc 2005;127:10388–95.
[8] Bertolazzi S, Wünsche J, Cicoira F, Santato C. Appl Phys Lett 2011;99:013301–3.
[9] Roberts ME, Queralt N, Mannsfeld SCB, Reinecke BN, Knoll W, Bao Z. Chem Mater 2009;21:2292–9.
[10] Facchetti A. Chem Mater 2011;23:733–58.
[11] Dang MT, Hirsch L, Wantz G. Adv Mater 2011;23:3597–602.
[12] Huo LJ, Zhang S, Guo X, Xu F, Li YF, Hou JH. Angew Chem 2011;123:9871–6.
[13] Hohenberg P, Kohn W. Phys Rev 1964;136:B864–71.
[14] Kohn W, Sham L. Phys Rev 1965;140:A1133–8.
[15] Jones RO, Gunnarsson O. Rev Mod Phys 1989;61:689–746.
[16] Baroni S, de Gironcoli S, Dal Corso A, Giannozzi P. Rev Mod Phys 2001;73:515–62.
[17] Sharma V, Pilania G, Rossetti GA, Slenes K, Ramprasad R. Phys Rev B 2013;87:134109.
[18] Wang CC, Ramprasad R. J Mater Sci 2011;46:90–3.
[19] Wang CC, Pilania G, Ramprasad R. Phys Rev B 2013;87:035103.
[20] Pilania G, Wang CC, Wu K, Sukumar N, Breneman C, Sotzing G, et al. J Chem Inf Model 2013;53(4):879–86.
[21] Sun Y, Boggs SA, Ramprasad R. Appl Phys Lett 2012;101:132906.
[22] Sun Y, Bealing C, Boggs SA, Ramprasad R. IEEE Electr Insul Mag 2013;29:8–15.
[23] Ranjan V, Buongiorno-Nardelli M, Bernholc J. Phys Rev Lett 2012;108:087802.
[24] Ranjan V, Yu L, Buongiorno-Nardelli M, Bernholc J. Phys Rev Lett 2007;99:047801.
[25] Huzayyin A, Boggs SA, Ramprasad R. IEEE Electr Insul Mag 2012;28:23–9.
[26] Huzayyin A, Boggs SA, Ramprasad R. IEEE Trans Dielectr Electr Insul 2010;17:920–5.
[27] Huzayyin A, Boggs SA, Ramprasad R. IEEE Trans Dielectr Electr Insul 2010;17:926–30.
[28] Huzayyin A, Boggs SA, Ramprasad R. Annual report of the conference on electrical insulation and dielectric phenomena; 2010. pp. 1–4.
[29] Jorgensen WL, Ulmschneider JP, Tirado-Rives J. J Phys Chem B 2004;108:16264–70.
[30] Wang JM, Wolf RM, Caldwell JW, Kollman PA, Case DA. J Comput Chem 2004;25:1157–74.
[31] Vanommeslaeghe K, MacKerell Jr AD. J Chem Inf Model 2012;52:3144–54.
[32] Vanommeslaeghe K, Prabhu Raman E, MacKerell Jr AD. J Chem Inf Model 2012;52:3155–68.
[33] Sun H. J Phys Chem B 1998;102:7338–64.
[34] Rigby D, Roe R. J Chem Phys 1987;87:7285–92.
[35] Bitsanis I, Hadziioannou G. J Chem Phys 1990;92:3827–47.
[36] Bennemann C, Paul W, Binder K. Phys Rev E 1998;57:843–51.
[37] Moreno M, Casalegno M, Raos G, Meille SV, Po R. J Phys Chem B 2010;114(4):1591–602.
[38] Pilania G, Wang CC, Jiang X, Rajasekaran S, Ramprasad R. Sci Rep 2013;3:2810.
[39] Sukumar N, Krein M, Luo Q, Breneman C. J Mater Sci 2012;47:7703–15.
[40] Hughes LD, Palmer DS, Nigsch F, Mitchell JBO. J Chem Inf Model 2008;48(1):220–32.
[41] Hart GLW, Blum V, Walorski MJ, Zunger A. Nat Mater 2005;4:391–4.
[42] Fischer CC, Tibbetts KJ, Morgan D, Ceder G. Nat Mater 2006;5:641–6.
[43] Saad Y, Gao D, Ngo T, Bobbitt S, Chelikowsky JR, Andreoni W. Phys Rev B 2012;85:104104.
[44] Rupp M, Tkatchenko A, Muller K, von Lilienfeld OA. Phys Rev Lett 2012;108:058301.
[45] Hautier G, Fisher CC, Jain A, Mueller T, Ceder G. Chem Mater 2010;22:3762–7.
[46] Hansen K, Montavon G, Biegler F, Fazli S, Rupp M, Scheffler M, et al. J Chem Theory Comput 2013;9(8):3404–19.
[47] Hammett LP. J Am Chem Soc 1937;59(1):96–103.
[48] Hansch C, Muir RM, Fujita T, Maloney PP, Geiger F, Streich M. J Am Chem Soc 1963;85:2817–24.
[49] Hansch C, Fujita T, editors. Classical and three-dimensional QSAR in agrochemistry. American Chemical Society symposium series. Washington: American Chemical Society; 1995.
[50] Taft RW. J Am Chem Soc 1952;74:3120–8.
[51] Katritzky AR, Lobanov VS, Karelson M. Chem Soc Rev 1995;24:279–87.
[52] Rabuffi M, Picci G. IEEE Trans Plasma Sci 2002;30:1939–42.
[53] Barshaw EJ, White J, Chait MJ, Cornette JB, Bustamante J, Folli F, et al. IEEE Trans Magn 2007;43:223–5.
[54] Tortai JH, Bonifaci N, Denat A, Trassy CJ. Appl Phys 2005;97:053304(1)–053304(9).
[55] Yuan X, Matsuyama Y, Chung TCM. Macromolecules 2010;43:4011–4.
[56] Chung TCM. Green Sustain Chem 2012;2:29–37.
[57] Gupta S, Yuan X, Chung TCM, Kumar S, Weiss RA. Macromolecules 2013;46:5455–63.
[59] Wang CC, Pilania G, Ramprasad R, Agarwal M, Misra M, Kumar S, et al. Appl Phys Lett 2013;102:152901.
[60] Grimme S. J Comput Chem 2006;27:1787–99.
[61] Liu CS, Pilania G, Wang CC, Ramprasad R. J Phys Chem A 2012;116:9347–52.
[62] Agarwal M, Misra M, Kumar S, Wang CC, Pilania G, Ramprasad R, et al. submitted.
[63] Baldwin AF, Ma R, Wang CC, Ramprasad R, Sotzing GA. J Appl Polym Sci 2013;130:1276–80.
[64] Lorenzini RG, Kline WM, Wang CC, Ramprasad R, Sotzing GA. Polymer 2013;54:3529–33.
[65] Gonze X, Lee C. Phys Rev B 1997;55:10355.
[66] Gonze X. Phys Rev B 1997;55:10337.
[67] Oganov AR, Glass CW. J Chem Phys 2006;124:244704.
[68] Lyakhov AO, Oganov AR, Valle M. Comput Phys Commun 2010;181:1623–32.
[69] Oganov AR, editor. Modern methods of crystal structure prediction. Berlin: Wiley-VCH; 2010, ISBN 978-3-527-40939-6; 2010.
[70] Goedecker S. J Chem Phys 2004;120:9911.
[71] Amsler M, Goedecker S. J Chem Phys 2010;133:224104.
[72] Pannetier J, Bassas-Alsina J, Rodriguez-Carvajal J, Caignaer V. Nature 1990;346:343–5.
[73] Kumar A, Wang CC, Ramprasad R. in preparation.
[74] Robertson J. Rep Prog Phys 2006;69:327–96.
[75] Robertson J. Solid State Electron 2005;49:283–93.
[76] Zhu H, Ramprasad R. Phys Rev B 2011;83:081416.
[77] Zhu H, Tang C, Fonseca RC, Ramprasad R. J Mater Sci 2012;47:7399–416.
[78] Cao Y, Boggs SA. IEEE Trans Dielectr Electr Insul 2005;12:690–9.
[79] Bealing CR, Ramprasad R. J Chem Phys 2013;139:174904.
[80] Laurent C. In: Proc. of 1998 IEEE 6th Intl. Conf. on conduction and breakdown in solid dielectrics Sweden 1998.
[81] von Hippel A. J Appl Phys 1937;8:815.
[82] Zener CM. Proc R Soc 1934;145:523–9.
[83] Frohlich H. J Appl Phys 1937;160:230.

Rampi Ramprasad is currently Professor of Materials Science and Engineering at the University of Connecticut, with joint appointments with the Departments of Physics, and Chemical and Biomolecular Engineering. After graduating with a PhD in Materials Science and Engineering from the University of Illinois at Urbana-Champaign in 1997, Prof. Ramprasad served as a technical staff member at Motorola's R&D division, before joining the University of Connecticut in 2004. Prof. Ramprasad's area of expertise is in the development and application of first principles materials computational tools, and more broadly in the utilization of such methods for the design and discovery of new materials, especially dielectrics and catalysts. He is the recipient of the Alexander von Humboldt Fellowship, the Max Planck Society Fellowship for Distinguished Scientists, and the United Technologies Corporation Professorship for Engineering Innovation.

Chenchen Wang received her B.S degree in Polymer Science and Engineering in 2008 from Zhejiang University, China. Presently, she is pursuing a Ph.D. degree in Materials Science and Engineering under the supervision of Prof. Ramprasad at the University of Connecticut. Her current research focuses on the design of polymer dielectrics for applications in high energy density capacitors using first principles computations and materials informatics.

Curt Breneman holds the position of Professor and Department Head in the Department of Chemistry & Chemical Biology at Rensselaer Polytechnic Institute (RPI), and is Director of the Rensselaer Exploratory Center for Cheminformatics Research (RECCR). After earning his Ph.D. in Physical Organic Chemistry at the University of California at Santa Barbara in 1987, Prof. Breneman was a post-doctoral research associate at Yale University until accepting a tenure-track position at RPI in 1989. Prof. Breneman is a Fellow of the American Chemical Society, and Chair of the ACS Division of Computers in Chemistry in 2010. For many years, he and his group have taken an active role in developing the fields of Predictive Cheminformatics in the area of drug discovery methods and created new Materials Informatics methods for aerospace, defense and energy applications.

Sanat Kumar received his ScD. in Chemical Engineering in 1987 from the Massachusetts Institute of Technology working with Professors Robert Reid and Ulrich Suter. He was a Director's post-doctoral fellow at the IBM Almaden research Center with Do Yoon, and then followed this with faculty appointments at Penn State University (1988–2002), Rensselaer Polytechnic Institute ('02–'06) and Columbia University ('06-). His research interests are in the field of polymers (nanocomposites, advanced capacitor materials, scattering methods) and biopolymers (protein–surface interactions). Kumar is a fellow of the APS and currently serves on the editorial advisory board of Macromolecules.

Ghanshyam Pilania is currently working as a postdoctoral research fellow in Materials Science and Technology Division at the Los Alamos National Laboratory. He received his BTech degree in Metallurgical and Materials Engineering from Indian Institute of Technology, Roorkee (Uttarakhand, India) in 2007 and his PhD degree from the University of Connecticut, Storrs (CT, USA) in 2012. Dr. Pilania carried out his graduate research work under the guidance of Prof. Ramprasad. His research interests include first principles design of advance functional materials for dielectric, catalytic and nuclear applications. He research also focuses on *ab initio* prediction of interesting phenomena at surfaces, interfaces and in nanostructures.

Steven Boggs was graduated with a B.A. in physics from Reed College and received his Ph.D. and MBA degrees from the University of Toronto in 1972 and 1987, respectively. He spent 12 years with the Research Division of Ontario Hydro and 6 years as Director of Engineering and Research for Underground Systems, Inc. Steve is presently Director of the Electrical Insulation Research Center of the University of Connecticut and Research Professor of Materials Science, Physics, and Electrical Engineering. Until recently, he was also an Adjunct Professor of Electrical Engineering at the University of Toronto. He has published widely in the areas of partial discharge measurement, high frequency phenomena in power apparatus, high field phenomena in solid dielectrics, capacitor technology, and SF_6 insulated systems. He was elected a Fellow of the IEEE for his contributions to the field of SF_6 insulated systems and received the 2010 IEEE Thomas W. Dakin "Distinguished Technical Contributions" award.